Characterization, Antimicrobial and Antioxidant evaluation of biofabricated silver nanoparticles from endophytic Pantoea anthophila

C. Nirmala
Vinayaka Mission's Kirupananda Variyar Engineering College
M Sridevi (drsridevimuruhan@gmail.com)
Vinayaka Mission's Kirupananda Variyar Engineering College https://orcid.org/0000-0002-4039-3393

Original Research Full Papers

Keywords: Pantoea anthophila, Endophytic bacterium, Silver Nanoparticles, Characterisation, Antimicrobial activity, Antioxidant activity

Posted Date: February 18th, 2021

DOI: https://doi.org/10.21203/rs.3.rs-205396/v1

Version of Record: A version of this preprint was published at Journal of Inorganic and Organometallic Polymers and Materials on March 29th, 2021. See the published version at https://doi.org/10.1007/s10904-021-01974-7.

Abstract

Endophyte mediated nanoparticles fabrication was emerging as a new frontier in nanomedicines that produce high biocompatible and functionalized silver nanoparticles. In this study, silver nanoparticles were successfully biosynthesized from the extracellular extract of endophytic bacterium *Pantoea anthophila* isolated from the stem of *Waltheria indica* for the first time. The synthesised nanoparticles were characterized by UV-Visible and Fourier Transform Infra-Red spectroscopy. The structural analysis is done by X-ray diffraction and the stability was studied by dynamic light scattering and particle size analyser. The size and shape were observed by Transmission Electron Microscope, Scanning Electron Microscope and Energy Dispersive X-Ray spectrum. Further, the nanoparticles were evaluated for antimicrobial and antioxidant properties. Synthesized nanoparticle showed a strong absorption band in the UV-Visible range at 410 nm. The average particle size was found to be 16.8 nm with spherical shaped, crystalline nature. Good zones of inhibition at various ranges were detected against a broad range of human pathogenic bacteria and fungi. A strong free radical scavenging activity of silver nanoparticles with IC_{50} values 30.75, 19.47, 34.59, 41.12, 27.24, 28.16, 36.21 µg/ml was obtained that was comparable to the reference. The study suggests that the silver nanoparticles can be biosynthesised from endophytic *P. anthophila* metabolites with significant therapeutic potential. With proper validation, the biosynthesised silver nanoparticles can be developed as a promising antiviral and anticancer drug candidate.

1. Introduction

The potential of human pathogens is rising alarmingly that leads to high death mortality rate. On the other hand, oxidative stress in cells increases the risk of diseases like acute lung injury, ageing, acute renal failure, cardiovascular diseases, diabetes, neurodegenerative diseases, cancer etc in humans [1,2]. Though wide-spectrum antibiotics are available they are least effective against the infectious agents. Products like carotenoids, vitamins and polyphenols from fruits and vegetables have the ability to modulate the oxidative stress [3,4]. Yet, low bioavailability and easy degradation during delivery limit their antioxidant activity [5]. The change in the way the prescribed drugs used for the treatment of various diseases or the development of novel candidates with high potency is the urgent need of the hour.

Nanotechnology, an emerging research area in science and technology has gained importance in biomedical, cosmetics, imaging, cancer therapy and targeted drug delivery [6,7]. The unique physiological properties, broad-spectrum activity, and low toxicity [8,9] acquired interest on nanoparticles, especially the nanosilver in development of antimicrobial [10], anti-plasmodial [11], anti-platelet [12], anti-tumour [13] and wound healing [14] pharmaceutical products. Nanoparticles are synthesized by physicochemical methods that are costly, highly toxic and time-consuming. An eco-friendly, sustainable technique has to be developed for the production of silver nanoparticles for various medical challenges. Biological sources such as plants, microbes (bacteria and fungi) and biomolecules (amino acids and vitamins) are recognized to reduce metal ions to nano metals [15,16]. The biomoieties in the natural extracts influence the microbial inhibitory and cellular toxicity of these green-synthesized nano metals.

Waltheria indica, a tropical medicinal plant is used traditionally in the treatment of many human ailments [17-19]. Endophytic groups colonizing the parts of *W. indica* are investigated and identified a novel bacterium *Pantoea anthophila* in the stem region. Endophytes have opened a new direction of exploration in nanoparticle synthesis. They colonise the internal tissues of plants, diversify between species, organs and play a key role in plant growth and defence. They are well known for the inimitable bioactive metabolites that act as the major source of drugs against various human diseases. Endophytic fungi from different plants are extensively studied for nanoparticle synthesis yet potency of endophytic bacteria in nano research is at the primitive stage [20,21]. This bottom-up approach may generate targeted nanomaterials at very high efficiency.

Based on these considerations, the present study has been designed to undertake the extracellular biosynthesis of silver nanoparticles (Pa-AgNPs) from *P. anthophila* and evaluate its therapeutic potential. To the best of our knowledge, this study is the first report on biofabrication, characterization, antimicrobial and antioxidant potentials of AgNPs biosynthesized using this bacterium. The study would also recommend the application of endophytic bacteria for nanoparticles synthesis in pharmaceutical applications as an alternative greener approach.

2. Materials And Methods

2.1 Chemicals, Endophytic Bacteria and Microbial strains

Analytical grade Silver nitrate ($AgNO_3$), tetracycline, kanamycin, nutrient agar, potato dextrose agar, Mueller-Hinton agar (Himedia Lab, Ltd., Mumbai, India) were used in the present study. The endophytic bacteria *Pantoea anthophila* (GenBank accession no. MN077163) identified earlier by 16S ribosomal RNA gene sequencing from *W. indica* were pure cultured and maintained in the laboratory. Bacterial pathogens such as Gram-positive *Staphylococcus epidermidis* (MTCC737), *Bacillus subtilis* (MTCC1133), *Staphylococcus aureus* (MTCC2940), Gram-negative *Escherichia coli* (MTCC40), *Proteus mirabilis* (MTCC425), *Salmonella typhi* (MTCC733), *Klebsiella pneumoniae* (MTCC2405) and fungal strains of *Aspergillus niger* (MTCC404), *Candida albicans* (MTCC183) and *Penicillium chrysogenum* (MTCC947) were obtained from Microbial Type Culture Collection (MTCC), Chandigarh.

2.2 Preparation of cell-free endophytic culture

P. anthophila (Pa) isolated from *W. indica* are subcultured and maintained in nutrient agar plates. A loopful of culture is inoculated in 100ml of Luria–Bertani broth at 37°C and placed in an orbital shaker at 200 rpm overnight. The cell-free extract was collected by centrifuging in a high-speed centrifuge (RM-03 Plus) (10,000rpm for 10min) and used immediately for AgNP synthesis.

2.3 Biosynthesis of Silver Nanoparticles

The 10 ml of bacterial cell free supernatant was mixed with 90ml of 1mM $AgNO_3$ solution for the biosynthesis of silver nanoparticles. The reaction mixture was incubated at 30°C for 24 hours in dark to

avoid any photochemical reactions. Simultaneously, the cell-free supernatant without silver nitrate was maintained as control. Formation of AgNPs was monitored at regular time intervals. Silver nanoparticles (Pa-AgNPs) formed were separated by centrifuging at 10,000rpm for 15 min. The water-soluble biological molecules, and other impurities are removed by washing the samples repeatedly (×3) with deionized water. The final mass of the AgNPs was collected and freeze-dried.

2.4 Biophysical characterization of Pa-AgNPs

The Pa-AgNPs are further characterized by UV-Visible spectroscopy, Dynamic Light scattering analysis (DLS), Zeta potential, Fourier Transform Infrared Spectroscopy (FTIR), X-ray Diffraction (XRD), Transmission Electron Microscopy (TEM), Scanning Electron Microscopy (SEM), Energy Dispersive of X-Ray spectrum (EDX).

The formation of AgNPs was confirmed by measuring the absorption spectra in UV-Visible spectroscopy (SHIMADZU 1800). The reaction mixture was scanned at the speed of 300 nm min^{-1} in 200–600 nm range. DLS analysis determines the particle size and distribution pattern of Pa-AgNP. Zeta sizer (Malvern Instruments Ltd., U.K ZS90) was used to determine the surface charge potential, the magnitude of charge attraction or repulsion and electrophoretic stability of Pa-AgNP.

The FTIR analysis was carried out to identify the functional biomolecules in the endophytic extract that reduces Ag+ to AgNPs and the capping agents that stabilize the nanoparticles. The Pa-AgNPs is scanned at the transmission mode ranging from 500 to 4000 cm^{-1} in a solid phase, at a resolution of 1 cm^{-1} using FTIR spectrophotometer (SHIMADZU, IR PRESTIGE 21). XRD pattern provides the details of the structure and composition of Pa-AgNPs. The sample was analyzed by Shimadzu XRD 6000 diffractometer operated at 40kV voltage, 30mA current in a scanning mode range of θ-2θ between 10 to 80 degrees with sampling pitch of 0.1000 degree equipped with a Cu Kα radiation.

The crystallite structure of the Pa-AgNP was measured using TEM (JEOL JEM 2100). The sample was placed on copper grids coated carbon films, dried at room temperature and analysed at 200kV. SEM shows the size, shape and surface morphological properties of Pa-AgNP synthesized from the endophytic extract. The nanoparticle was observed in SEM (JEOL– JSM 6390) at a voltage of 15–20kV at different magnifications. The atomic composition of Pa-AgNP was confirmed by EDX analysis (Oxford instrument, INCA PentaFET x3) coupled with SEM.

2.5 Antimicrobial Screening of Pa-AgNPs

The antimicrobial activities of the synthesized Pa-AgNPs were analysed by Agar well diffusion method [22]. The microbial strains *S. epidermidis, B. subtilis, S. aureus, E. coli, P. mirabilis, S. typhi, K. pneumonia* at exponential growth phase were cultured in Muller Hinton agar plates. Six wells of about 5mm diameter were bored in each agar plates. Different concentrations of Pa-AgNPs (25µg/mL, 50µg/mL, 75µg/mL, 100µg/mL), 10µg/mL of dimethyl sulfoxide (DMSO) (negative control) and Tetracycline (positive control) were added to the wells.

The fungal strains *A. niger, C. albicans* and *P. chrysogenum* in potato dextrose agar are utilised for antifungal activity testing of Pa-AgNPs by agar well diffusion method, where Kanamycin (10µg/mL) is used as a positive control. The plates were incubated for 24 hours at 37°C to observe the clear zones of inhibition (ZOI). The diameter of clear zones was measured and recorded.

2.6 Antioxidant efficacy of Pa-AgNPs

2.6.1 1, 1-diphenyl-2- picrylhydrazyl (DPPH) radical scavenging assay

DPPH radical scavenging assay potential of Pa-AgNPs was assayed [23] at different concentrations (10, 20, 30, 40 & 50 µg/ml) of Pa-AgNPs and standard Ascorbic acid. In methanol solution, dissolved 50µl of 0.659 mM DPPH, added to the samples and the volume is made up to one with double distilled water. The tubes were incubated in dark at 25ºC for 20 minutes and the absorbance was recorded at 510 nm using Shimadzu UV 1800 spectrophotometer. The % inhibition (I%) was calculated as (I%) = 100 x $(A_0-A_1)/A0$, Where A_0 is the absorbance of the control, A_1 is the absorbance of the Pa-AgNPs and standard.

2.6.2 Nitric oxide radical scavenging assay

At physiological pH, in aqueous solution, sodium nitroprusside generates nitric oxide that interacts with oxygen to produce nitrite ions, which can be measured in the presence of Griess reagent [23]. To various concentrations (10-50µg/ml) of Pa-AgNPs and standard ascorbic acid, added 50µl of 10mM sodium nitroprusside dissolved in 0.5M phosphate buffer (pH 7.4) and incubated under fluorescent light at room temperature for 15 minutes. Added 125µl of Griess reagent, the tubes were incubated again at room temperature for 10 minutes and the absorbance was recorded at 546nm.

2.6.3 Hydrogen peroxide (H_2O_2) scavenging assay

The ability of the Pa-AgNPs to scavenge H_2O_2 was determined according to the method of Nabavi et al. [24]. 0.6ml of 40mM of H_2O_2 was prepared using 50mM phosphate buffer (pH 7.4) and added to varied concentrations (10-50µg/ml) of Pa-AgNPs and standard ascorbic acid. The tubes were incubated for 10 minutes and the absorbance was noted at 230 nm.

2.6.4 Total antioxidant capacity assay

The total antioxidant capacity assay was determined [25] by adding 1ml of reagent solution containing sulphuric acid (0.6M), sodium phosphate (28mM) and Ammonium molybdate (4mM) to Pa-AgNPs and standard ascorbic acid (10-50 µg/ml). The tubes were capped, incubated at 95ºC for 90 minutes in a thermal block and then cooled to room temperature, the absorbance was measured at 695 nm.

2.6.5 2,2'-Azino-bis-3-ethyl benzothiozoline-6-sulfonic acid (ABTS) radical scavenging activity

The assay is based on the scavenging of light by ABTS radicals. An antioxidant that donates a hydrogen atom will quench the stable free radical which can be quantified spectrometrically at 734nm [23]. 200µl

of 70mM potassium persulphate and 50ml of 2mM ABTS were mixed before 2hours. To the 0.5ml of various concentrations (10-50µg/ml) of Pa-AgNPs and standard ascorbic acid, 0.3ml of ABTS radical cation and 1.7ml of phosphate buffer (pH 7.4) was added and the absorbance was measured.

2.6.6 Reducing Power Assay

Different concentrations (10-50 µg/ml) of Pa-AgNPs solution were mixed with 2.5ml of 200mM phosphate buffer (pH 6.6) and 1% potassium ferricyanide each. Incubated at 50ºC for 20 min, the mixture was cooled rapidly. Subsequently, added 2.5ml of 10% Trichloroacetic acid and centrifuged at 3000 rpm for 10 min. The supernatant (5ml) with an equal amount of distilled water were mixed and added to 1ml of 0.1% ferric chloride. Using ascorbic acid as a standard, the absorbance was measured at 700 nm [26].

2.6.7 Superoxide (O_2^-) radical Scavenging Assay

The superoxide scavenging activity of the Pa-AgNPs was assayed by the reduction of nitro blue tetrazolium (NBT) [27]. To Pa-AgNPs solution (10-50µg/ml), 3ml Tris–HCl buffer (16 mM, pH 8), 1ml NBT (50µM), 1ml Nicotinamide Adenine Dinucleotide (78µM) and 1ml phenazine methosulfate (PMS) solution (10µM) were mixed and kept for 5 min at 25°C. The absorbance was recorded at 560 nm. Ascorbic acid was used as standard.

Inhibition % versus concentration curve was plotted for each assay and the concentration of sample required for 50% inhibition was determined and expressed as IC_{50} value. The lower IC_{50} value indicates a high antioxidant capacity.

3. Results And Discussion

3.1 Endophytic *Pantoea anthophila*

P. anthophila was previously reported in eucalyptus and maize and also found to cause infections in *Impatiens balsamina*, *Tagetes erecta* and *Clausena lansium* [28,29]. The multidimensional property of endophytes may produce stable nanoparticles with high medicinal potency, hence the extracelluar metabolite rich broth of *P. anthophila* are utilised for Pa-AgNPs synthesis.

3.2 Biosynthesis and Characterization studies of Pa-AgNPs

3.2.1 UV–visible spectroscopy

The formation of AgNPs was observed from the colour change of endophytic extract mixed with $AgNO_3$ from yellow to dark brown after 24 hours (Fig. 1b). At the same time, no colour change was detected in the control (Fig. 1a). Further, the reaction mixture recorded a maximum absorption peak at the wavelength 410nm (Fig. 2) that confirms the formation of AgNPs. The colour change in bacterial extract on the addition of $AgNO_3$ and the characteristic absorption peak centred at 410nm may be due to

Plasmon resonance peak that confirms the formation of AgNPs in the extract. Similar peaks were also reported in studies [30-32] relevant to the biosynthesis of AgNPs.

3.2.2 DLS and Zeta potential analysis

The DLS analysis (Fig. 3) showed that the average size of Pa-AgNPs was 16 nm and the size varies from 10-24 nm. The zeta potential of the Pa-AgNPs was found as a sharp peak at 5.30mV (Fig.4) which indicates that the surface of synthesized nanoparticles was stable, positively charged and have strong agglomeration and precipitation. The results are in concurrence with preceding scientific reports of AgNPs [33,34].

3.2.3 FTIR spectroscopy study

FTIR spectrum displayed the presence of predominant bands at 3423.65, 1633.71, 1022.27, 607.58 cm^{-1} (Fig. 5). The peak at 3423.65cm^{-1} corresponds to the O-H stretching vibrations of water molecules. The bands at 1633.71cm^{-1} show C=C stretching vibrations of non-conjugated, disubstituted alkene group. The band at 1022.27 cm^{-1} can be assigned to medium C–N stretching vibrations of amines signifying the presence of amino acid. The peak obtained at 607.58 cm^{-1} regions could be attributed to alkyl halides stretching. The results obtained coincide with the earlier findings of AgNPs FTIR prediction [35,36] that revealed the presence of hydroxyl, alkene and amine groups in the bacterial extract acting as reducing, capping and stabilizing agents of silver ions.

3.2.4 XRD analysis

XRD analysis showed the strongest Braggs peaks at 2θ values of 38.30°, 44.62°, 65.01° and 77.27° (Fig. 6). These peaks are conferred to 100, 200, 220 and 311 planes of a face centred cubic structure of Pa-AgNPs that agrees with the JCPDS file no. 87-0720 for silver. The crystallite domain sizes of Pa-AgNPs were calculated using Debye-Scherrer formula [37] $D = 0.94\lambda / \beta\cos\theta$, where D is the average crystallite domain size perpendicular to the reflecting planes, λ is the X-ray wavelength, β is the full width at half maximum (FWHM), and θ is the diffraction angle. The average crystallite size was found to be 16.8 nm that was in close agreement with DLS analysis. No secondary peaks were observed, hence the crystalline stable AgNP formation from the endophytic extract is justified with the previous XRD data [31, 38, 39].

3.2.5 TEM measurement

The antimicrobial activity of AgNPs is greatly influenced by their shape and size [40]. The TEM micrographs (Fig.7) exposed that Pa-AgNPs have a spherical shape with an average size of 20±1.1 nm. They were found to be circular aggregates with smooth edges that are not in direct contact. This indicates that the Pa-AgNPs are stabilised by capping agents from the endophytic extract. Selected area electron diffraction (SAED) pattern (Fig. 8) confirms the polycrystalline nature for a face centred cubic structure of synthesized silver nanoparticles. The result was nearly in congruence with DLS analysis and XRD data of the sample. The result obtained was also identical to earlier reports of green synthesized

AgNPs [20,41]. Thus the small size of nanoparticles enhances the reactivity and catalytic activity in various applications.

3.2.6 SEM and EDX

The SEM micrograph (Fig. 9) showed that the Pa-AgNPs were spherical shaped, nonuniform polydispersed with an average size of 50 nm. The smaller particles may aggregate to give the large-size appearance of nanoparticles [41]. The large particle size depicted in SEM compared to DLS, XRD and TEM may be due to the difference in sample preparation and the presence of various forces of interaction in the solution [42,43]. The EDX profile (Fig. 10) showed a sharp absorption peak between 3–4keV that is typical to the presence of metallic AgNPs along with iron. The weight of silver was found to be 41.77 %, thus confirms Pa-AgNPs was successfully biosynthesized from endophytic bacterial extracts [31,42].

3.3 Antimicrobial Screening of Pa-AgNPs

Pa-AgNPs showed promising antimicrobial activity in a dose-dependent manner. Significant antibacterial activity with minimum ZOI of 5 mm was observed against *S. aureus, S. epidermidis, P. mirabilis* and 4 mm against *E. coli, S. typhi and K. pneumonia* at 25µg/mL. The maximum ZOI of 7 mm was observed at 100µg/mL for all pathogens, while *B. Subtilis* exhibited low activity (5 mm) (Fig. 11). The diameters of the ZOI for the tested pathogens are illustrated in Fig. 12. Hu et al. [44] observed similar ZOI against *S. aureus, B. cereus, S. enterica, P. aeruginosa* and *E. coli* by Tp-AgNPs synthesized from endophytic fungi *Talaromyces purpureogenus*. The results obtained confirms the broad spectrum activity of Pa-AgNPs against both Gram-positive and Gram-negative bacteria that were compared with antibiotic controls.

P. chrysogenum and *C. albicans* was inhibited at 4 mm (100µg/mL) and 7 mm to 11 mm (dose-dependent) (Fig. 13) respectively, where as there is no ZOI for *A. niger*. Hence, the growth of *C. albicans* was greatly controlled than *Penicillium* and *Aspergillus.* The antimicrobial effect of Pa-AgNPs against *C. albicans* was strong compared to the crude *W.indica* leaf extracts reported by Koma et al. [17]. The results obtained justifies potent microbicidal activity of Pa-AgNPs that were also relevant with the reported literatures [45-47] of AgNPs. Presence of charge, size, shape, concentration, dissolution rate, species type, tolerance and time of exposure may attribute to the antimicrobial property of AgNPs [21, 48-50].

To the best of our knowledge, the present study is the first scientific report on the potential of Pa-AgNPs against the human pathogenic microbes. The study can be extended against MDR bacteria, other clinical pathogens and pandemic viruses to overcome the current challenging situations. The low cost biosynthesised AgNPs can also be used to reduce the secondary risks caused in COVID-19 patients.

3.4 Antioxidant efficacy of Pa-AgNPs

The DPPH radical, H_2O_2 radical and ABTS radical scavenging activity of Pa-AgNPs increased in a dose-dependent manner from 37.69 ± 0.69 % to 61.23 ± 0.48 %; 28.85 ± 0.29 to 57.34 ± 0.73 % and 34.03 ± 0.65 % to 68.9 ± 0.15 % respectively at the concentration from 10 to 50µg/mL, which is comparable with

standard ascorbic acid that had 20.34 ± 0.75 % to 65.54 ± 0.55 %., 31.05 ± 0.34 to 65.21 ± 0.65 %, 33% ± 0.25 to 69 ± 0.35 % of inhibition respectively (Fig. 14a, 14d, 14e).

The reducing power of compounds also increased analogous to their antioxidant ability. The reductive capability of the Pa-AgNPs increased from 39.39 ± 3.6 to 64.07 ± 0.58 %, while it is 37.17 ± 1.2 % to 58.06 ± 1.6 % at the same concentration for standard (Fig. 14f).

Pa-AgNPs scavenges the superoxide and nitric oxide radical up to 63.18 ± 0.48 % and 68.68 ± 0.68 % at 50µg/mL that was comparable to the scavenging effect of ascorbic acid 55% ± 0.23 and 70.94 ± 3.6 % at 50µg/mL (Fig. 14g, 14b). The total antioxidant capacity of the Pa-AgNPs showed the highest inhibition of 63.54 ± 4.1 % at 50µg/mL, while the reference showed 69.76 ± 0.61% at the same concentration (Fig. 14c).

Thus Pa-AgNPs have strong DPPH radical scavenging activity, nitric oxide radical scavenging activity and reducing power activity when compared to the standard. In H_2O_2 radical scavenging assay, total antioxidant capacity assay and ABTS radical scavenging assay, standard ascorbic acid showed strong antioxidant activity than Pa-AgNPs. The superoxide radical scavenging activity was similar for both Pa-AgNPs and standard. Netala et al. [51] observed 55.62 ± 0.25 % of inhibition in DPPH radical scavenging assay at 50µg/mL by AgNPs synthesised by endophytic fungi that was lower than that obtained by Pa-AgNPs. Also the nitric oxide radical, H_2O_2 radical scavenging and reducing assay of biogenic silver nanoparticles reported at 50µg/mL was lower than that obtained by Pa-AgNPs [52]. The results were also in line with the previous reports [53, 54]. The comparison of IC_{50} in each assay is illustrated in Table 1 and the lower IC_{50} values shows the higher antioxidant potency of the Pa-AgNPs.

Table 1: Antioxidant Activity of Pa-AgNPs

S.No.	Parameters	IC_{50} Value (µg/ml)	
		Pa-AgNPs	Ascorbic acid
1.	DPPH radical scavenging assay	30.75	34.60
2.	NO radical scavenging assay	19.47	22.87
3.	Total antioxidant capacity assay	34.59	21.84
4.	H_2O_2 radical scavenging assay	41.12	35.06
5.	ABTS radical scavenging assay	27.24	26.88
6.	Reducing power assay	28.16	32.96
7.	Superoxide radical scavenging assay	36.21	37.50

Thus Pa-AgNPs was proved to have strong antioxidant activity that may occur due to the adsorption of functional groups from the endophytic extract on the surface of Pa-AgNPs [55]. The excellent radical scavenging activity of Pa-AgNPs admit them to be used as potent antioxidants or as a valuable component of antioxidant formulations in biomedical and pharmaceutical fields [56]. The antioxidant property can be evaluated *in vivo* models prior to human applications in the treatment of various oxidative stress-related to degenerative diseases.

4. Conclusions

In the present study, the endophytic bacterium *P. anthophila* isolated from the stem of *W. indica* was used for extracellular biosynthesis of AgNPs. Structural characterization showed the optimal formation of Pa-AgNPs with crystalline nature at 410 nm UV-visible spectra between 16 to 20 nm size with positive surface potential. The bacterial metabolites formed a stable capping moiety around AgNPs and the elemental composition of Pa-AgNPs was also confirmed. They exhibited potential antimicrobial activity against 10 different pathogens. Higher antioxidant activity of Pa-AgNPs was also confirmed by DPPH, NO, H_2O_2, ABTS, superoxide radical scavenging assay, total antioxidant capacity assay and reducing power assay. Thus endophytic *P. anthophila* mediated biosynthesis of AgNPs prevails as eco-friendly, cost-effective and substantial method with increased potency of applications in nanomedicine. Further, the efficiency and mechanism of Pa-AgNPs to establish as anticancer and antiviral agents will be evaluated in future to ascertain that green synthesized AgNPs are an optimistic therapeutic agent in the trending era of biomedicines.

Abbreviations

AgNPs	Silver nanoparticles
Pa-AgNPs	Silver nanoparticles biosynthesized from *Pantoea anthophila*
rpm	revolution per minute
mM	milli molar
DLS	Dynamic Light scattering analysis
FTIR	Fourier Transform Infrared Spectroscopy
XRD	X-ray Diffraction
SEM	Scanning Electron Microscopy
TEM	Transmission Electron Microscopy
EDX	Energy Dispersive of X-Ray spectrum

Ag+	Silver ions
DMSO	Dimethyl sulfoxide
DPPH	1, 1-diphenyl-2- picrylhydrazyl
NO	Nitric oxide
H_2O_2	Hydrogen peroxide
ABTS	2,2'-Azino-bis-3-ethyl benzothiozoline-6-sulfonic acid
NBT	Nitro blue tetrazolium
PMS	Phenazinemethosulfate
COVID	Corona Virus Disease
IC_{50}	50% inhibition

Declarations

Funding

No funding was received for conducting this study.

Conflicts of interest/ Competing interests

The authors declare that there is no Competing interests.

Ethics approval

This article does not contain any studies with human participants or animals performed by the authors.

Consent to participate - Not applicable

Consent for publication - Not applicable

Availability of data and material

All data generated or analyzed during this study are available upon request.

Code availability - Not applicable

Authors' contributions

CN had collected all the literatures, samples and undergone the research work, analyzed, and prepared the complete manuscript. MS has critically reviewed the article for improvement. All authors have read and approved the final manuscript.

Acknowledgements

The authors gratefully acknowledge Department of Biotechnology, Vinayaka Mission's Kirupananda Variyar Engineering College, Salem and Acme ProGen Biotech (India) Private Limited, Salem for providing the essential facilities to carry out the research.

References

1. Gupta, S.P. Authimoolam, J.Z. Hilt, T.D. Dziubla, Actabiomaterialia. (2015) https://doi.org/10.1016/j.actbio.2015.08.039.
2. Sharpe, D. Andreescu, S. Andreescu, Am Chem Soc. (2011) https://doi.org/10.1021/bk-2011-1083.ch008.
3. Y. Lim, T.T. Lim, J.J. Tee, Food Chem. (2007) https://doi.org/10.1016/j.foodchem.2006.08.038.
4. A. Anagnostopoulou, P. Kefalas, V.P. Papageorgiou, A.N. Assimopoulou, D. Boskou, Food Chem. (2006) https://doi.org/10.1016/j.foodchem.2004.09.047
5. K. Verma. J Pharm Res.**8**, 7 (2014).
6. Ahmed, M. Ahmad, B.L. Swami, S. Ikram, J Adv Res. (2016) https://doi.org/10.1016/j.jare.2015.02.007.
7. Saifuddin, C.W. Wong, A.A. Yasumira, J Chem. **6**, 1 (2009).
8. Coe, W.K. Woo, M. Bawendi, V. Bulović V, Nature. (2002) https://doi.org/10.1038/nature01217.
9. Bruchez, M. Moronne, P. Gin, S. Weiss, A.P. Alivisatos, Sci. (1998) https://doi.org/10.1126/science.281.5385.2013
10. K. Singh, K. Bhardwaj, P. Dubey, A. Prabhune, RSC adv. (2015) https://doi.org/10.1039/C4RA17233G.
11. Mishra, N.K. Kaushik, M. Sardar, D. Sahal, Colloid Surface B. (2013) https://doi.org/10.1016/j.colsurfb.2013.06.036
12. N. Krishnaraj, S. Berchmans, RSC adv. (2013) https://doi.org/10.1039/C3RA41246F.
13. Castro-Aceituno, S. Ahn,S.Y. Simu, P. Singh, R. Mathiyalagan, H.A. Lee, D.C. Yang, Biomed Pharmacother. (2016) https://doi.org/10.1016/j.biopha.2016.09.016.
14. Rigo, L. Ferroni, I. Tocco, M. Roman, I. Munivrana, C. Gardin, W.R. Cairns, V. Vindigni, B. Azzena, C. Barbante, B. Zavan, Int J Mol Sci. (2013) https://doi.org/10.3390/ijms14034817.
15. C. Chen, Z.H. Lin, X.X. Ma, Lett Appl Microbiol. (2003) https://doi.org/10.1046/j.1472-765X.2003.01348.x.
16. Ahmad, P. Mukherjee, S. Senapati, D. Mandal, I.M. Khan, R. Kumar, M. Sastry, Colloid Surface B. (2003) https://doi.org/10.1016/S0927-7765(02)00174-1.

17. S. Koma, O.A. Fatokun, O.A. Theophilus, Biomed Sci. (2017) https://doi.org/10.11648/j.bs.20170305.11.
18. Musa, M. Musah, H. Yerima, N.B. Erena, Journal of Advance Research in Applied Science. 3, 4 (2016).
19. Nirmala, M. Sridevi,Futur J Pharm Sci.**7** (2021) https://doi.org/10.1186/s43094-020-00174-3
20. S. Devi, S.R. Joshi, J Microsc Ultrastruct. (2015) http://dx.doi.org/10.1016/j.jmau.2014.10.004.
21. Monowar, M. Rahman, S.J. Bhore, G. Raju, K.V. Sathasivam, Mole. (2018) https://doi.org/10.3390/molecules23123220.
22. Patil Shriniwas, Biochem Biophys. Rep. **10**, 76 (2017).
23. K. Jain, R.K. Agrawal, Asian J Exp Sci. **22**, 3 (2008).
24. M. Nabavi, M.A. Ebrahimzadeh, S.F. Nabavi, A. Hamidinia, A.R. Bekhradnia, Pharmacologyonline. **2** (2008).
25. Prieto, M. Pineda, M. Aguilar, Anal Biochem. (1999) https://doi.org/10.1006/abio.1999.4019.
26. C. Yen, P.D. Duh, J Am Oil Chem Soc. (1993) https://doi.org/10.1007/BF02552711.
27. Liu, V.E. Ooi, S.T. Chang, Life Sci. (1997) https://doi.org/10.1016/S0024-3205(97)00004-0.
28. N. Zhou, S.Y. Liu, Y.F. Chen, L.S. Liao, Plant Dis. (2015) https://doi.org/10.1094/PDIS-10-14-1025-PDN.
29. L. Brady, I. Cleenwerck, S.N. Venter, K. Engelbeen, P. De Vos, T.A. Coutinho, Int J Syst Evol Micr. (2010) https://doi.org/10.1099/ijs.0.017301-0.
30. Mie, M.W. Samsudin, L.B. Din, A. Ahmad, N. Ibrahim, S.N. Adnan, Int J Nanomedicine. (2014) https://doi.org/10.2147/IJN.S52306.
31. Singh, K. Jyoti, A. Patnaik, A. Singh, R. Chauhan, S.S. Chandel, J Genet Eng Biotechnol. (2017) https://doi.org/10.1016/j.jgeb.2017.04.005.
32. M. Attia, M.S. Abdelfatah, M.M. Mossad, J Phys: Conf Ser. (2017) https://doi.org/10.1088/1742-6596/869/1/012036.
33. Selvarani, P.V. Moorthi, P. Saranya, M. Abirami, Kenkyu J Nanotechnol Nanosci.1 (2015). 13
34. A. Ali, R. Yahya, S.D. Sekaran, R. Puteh, Adv Mater Sci Eng. (2016) https://doi.org/10.1155/2016/4102196.
35. Singh, V. Rathod, S. Ninganagouda, J. Hiremath, A.K. Singh, J. Mathew, Bioinorg Chem Appl. (2014) https://doi.org/10.1155/2014/408021.
36. A. Roseline, M. Murugan, M.P. Sudhakar, K. Arunkumar, Environ Technol Innovation. (2019) https://doi.org/10.1016/j.eti.2018.10.005.
37. D. Cullity, Elements of X-ray diffraction, 2nd edn. (Reading, MA: Addison-Wesley Publishing Company, Inc., 1978).
38. Gnanadesigan, M. Anand, S. Ravikumar, M. Maruthupandy, V. Vijayakumar, S. Selvam, M. Dhineshkumar, A.K. Kumaraguru. Asian Pac J Trop Med. (2011) https://doi.org/10.1016/S1995-7645(11)60197-1.

39. Y. Dong, M.P. NarsingRao, M. Xiao, H.F. Wang, W.N. Hozzein, W. Chen, W.J. Li, Front Microbiol. (2017) https://doi.org/10.3389/fmicb.2017.01090.
40. Kumari, S. Pandey, V.P. Giri, A. Bhattacharya, R. Shukla, A. Mishra, C.S. Nautiyal, Microb Pathogen. (2017) https://doi.org/10.3390/molecules23123220.
41. Devaraj, P. Kumari, C. Aarti, A. Renganathan, J Nanotechnol. (2013) https://doi.org/10.1155/2013/598328.
42. Banerjee, D. Nath,Nanosci Technol. **2**, 1 (2015).
43. A. Otunola, A.J. Afolayan, Biotechnol Biotechnol Equip. (2018) https://doi.org/10.1080/13102818.2018.1448301.
44. Hu, T.J. Kandasamy Saravanakumar, M.H. Wang, Int J Nanomedicine. (2019) https://doi.org/10.2147/IJN.S200817.
45. Al-Zubaidi, A. Al-Ayafi, H. Abdelkader, J Nanotechnol Res. (2019) https://doi.org/10.26502/jnr.2688-8521002.
46. Perween, H.M. Khan, N. Fatima, J Microbiol Exp. 7, 1 (2019).
47. K. Mishra, K.N. Tiwari, R. Saini, P. Kumar, S.K. Mishra, V.B. Yadav, G. Nath, J Inorg Organomet Polym. (2020). https://doi.org/10.1007/s10904-019-01392-w
48. Hamouda, A. Myc, B. Donovan, A.Y. Shih, J.D. Reuter, J.R. Baker, Microbiol Res. (2001) https://doi.org/10.1078/0944-5013-00069.
49. Sondi, B. Salopek-Sondi, J Colloid Interface Sci. (2004) https://doi.org/10.1016/j.jcis.2004.02.012.
50. Dibrov, J. Dzioba, K.K. Gosink, C.C. Häse, Antimicrob Agents Chemother. (2002) https://doi.org/10.1128/AAC.46.8.2668-2670.2002.
51. R. Netala, V.S. Kotakadi, P. Bobbu, S.A. Gaddam, V. Tartte, 3 Biotech. (2016) https://doi.org/10.1007/s13205-016-0433-7.
52. Bhakya, S. Muthukrishnan, M. Sukumaran, M. Muthukumar, Appl Nanosci. (2016) https://doi.org/10.1007/s13204-015-0473-z.
53. Hemashekhar, C. Chandrappa, M. Govindappa, N. Chandrasekhar, N. Ganganagappa, Y. Ramachandra, Inter J Eng Res Appl. (2017) https://doi.org/10.9790/9622-0708011724. 14
54. H. Ramamurthy, M. Padma, R. Mareeswaran, A. Suyavaran, M.S. Kumar, K. Premkumar, C. Thirunavukkarasu, Colloids Surf B. (2013) https://doi.org/10.1016/j.colsurfb.2012.09.025.
55. K. Keshari, R. Srivastava, P. Singh, V. B. Yadav, G. Nath, J Ayurveda Integr Med. (2020) https://doi.org/10.1016/j.jaim.2017.11.003.
56. P. Chandrappa, M. Govindappa, N. Chandrasekar, S. Sarkar, S. Ooha, R. Channabasava, Adv Nat Sci Nanosci. (2016) https://doi.org/10.1088/2043-6262/7/2/025016

Figures

Figure 1

a endophytic extract Control. b endophytic extract mixed with AgNO3

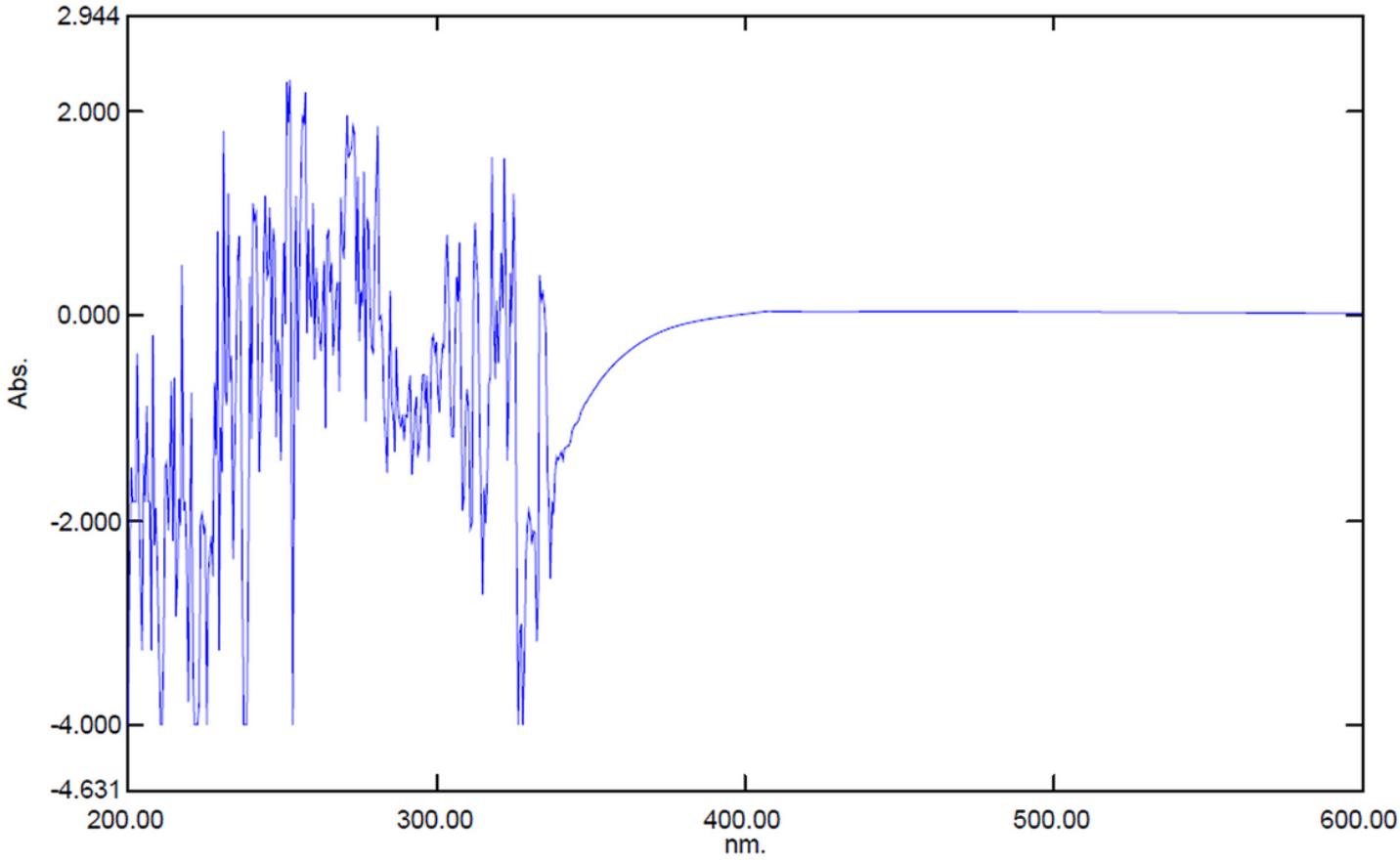

Figure 2

UV–visible absorption spectrum

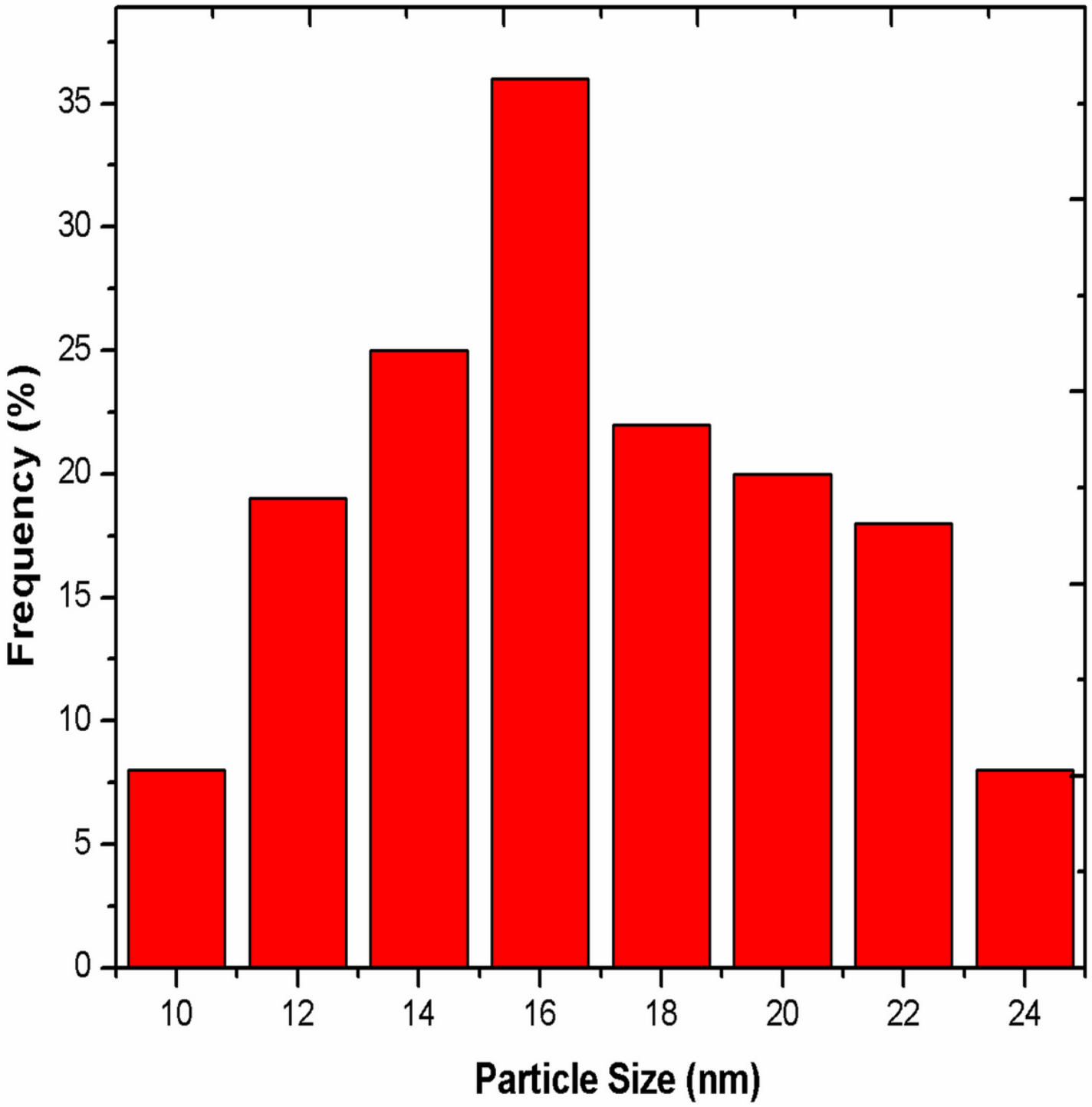

Figure 3

DLS analysis

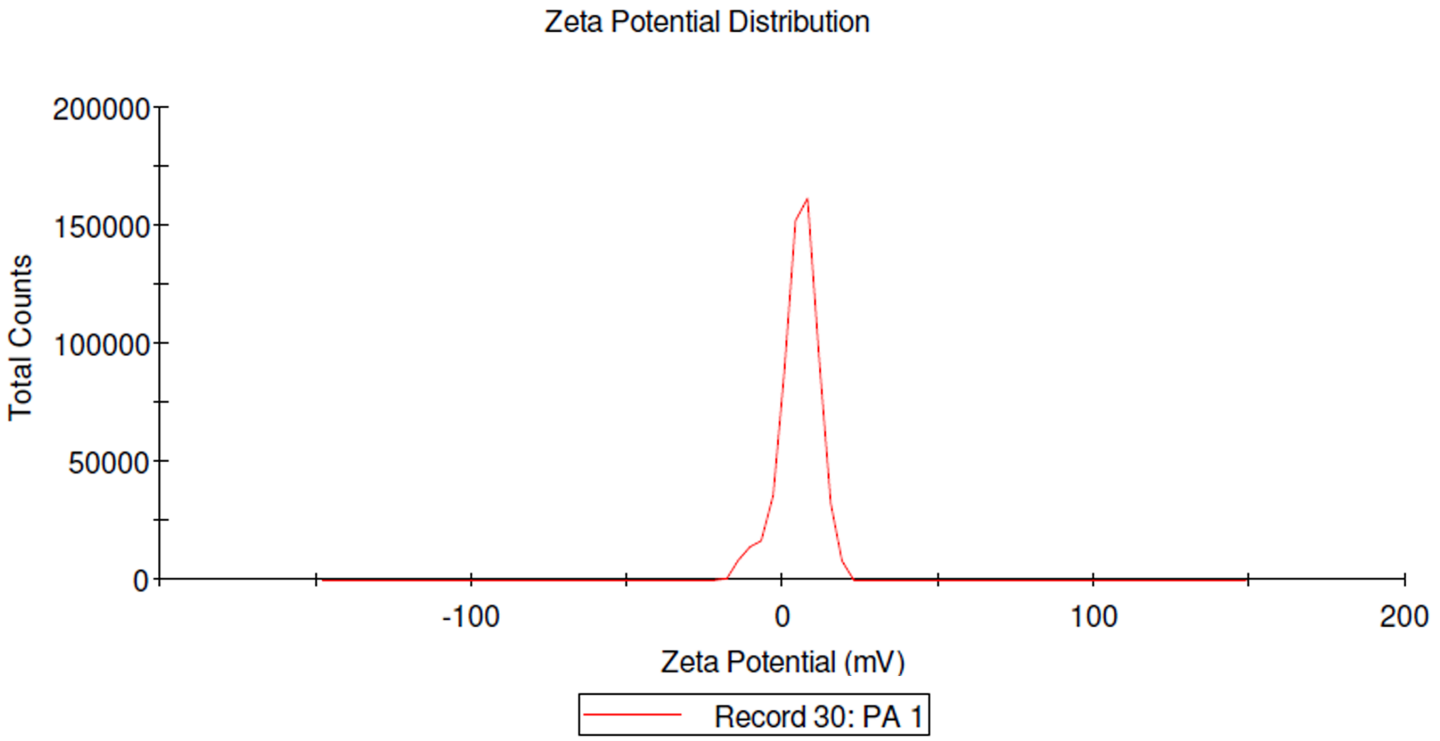

Figure 4

Zeta potential of Pa-AgNPs

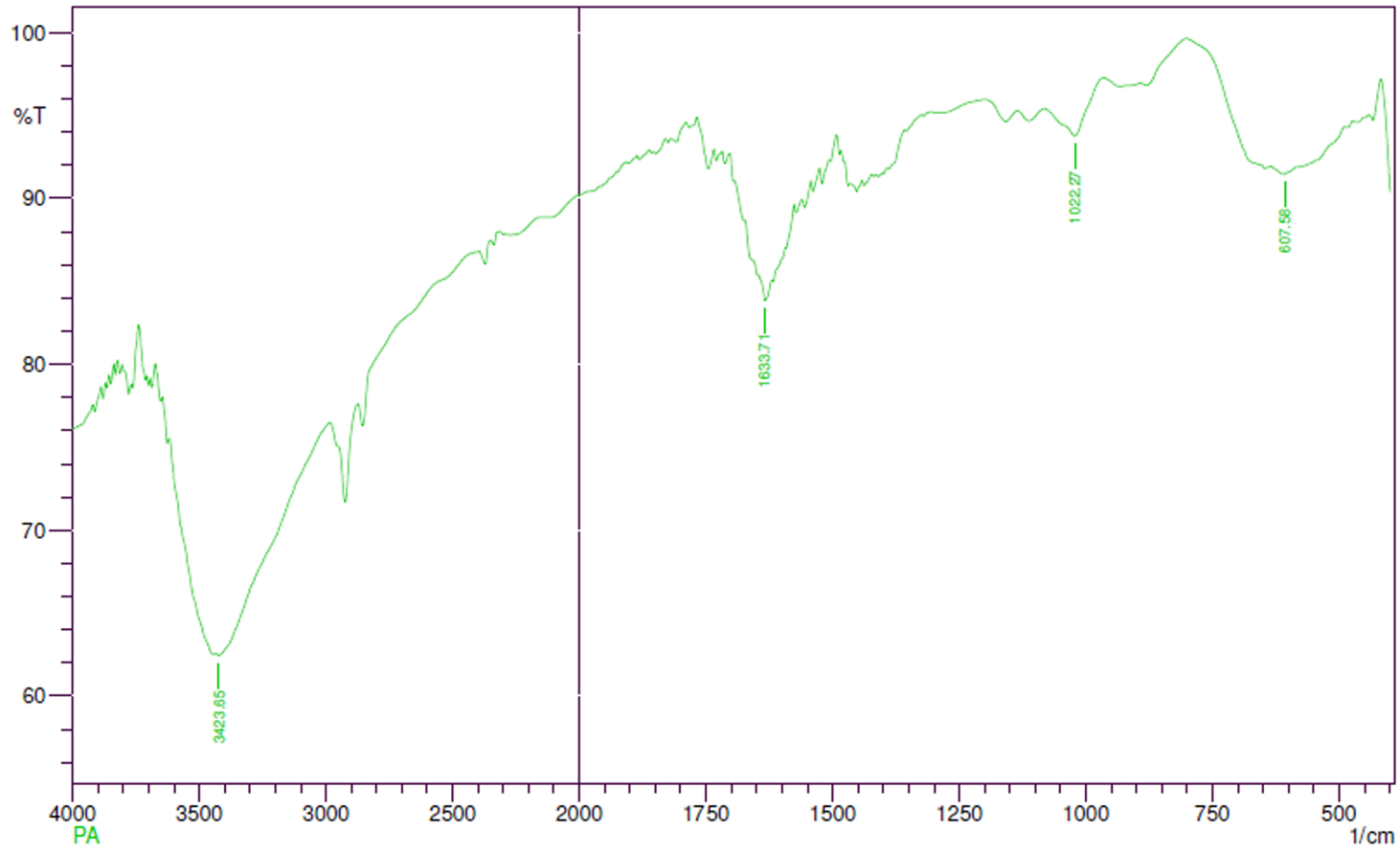

Figure 5

FTIR spectrum of Pa-AgNPs

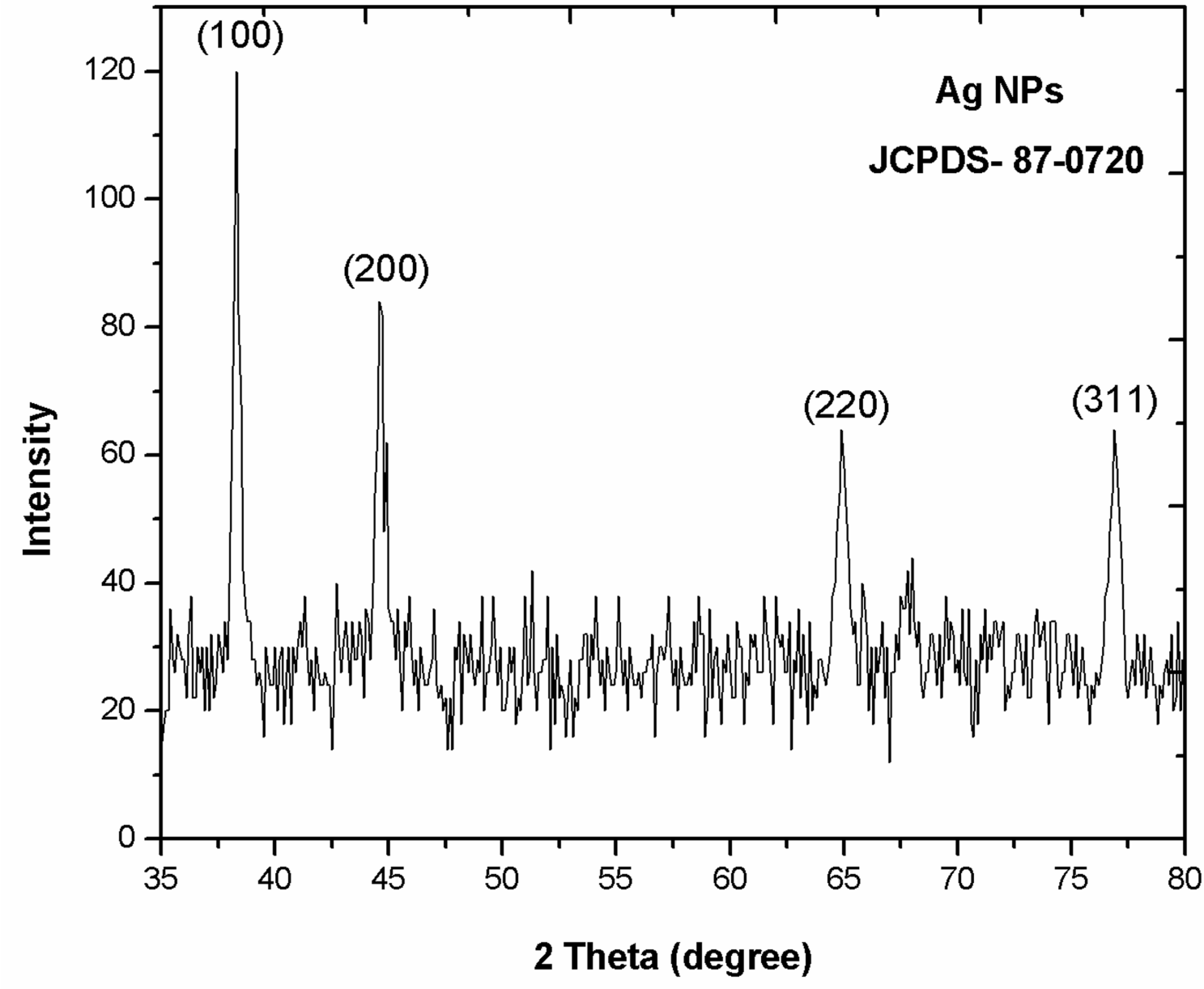

Figure 6

XRD analysis of Pa-AgNPs

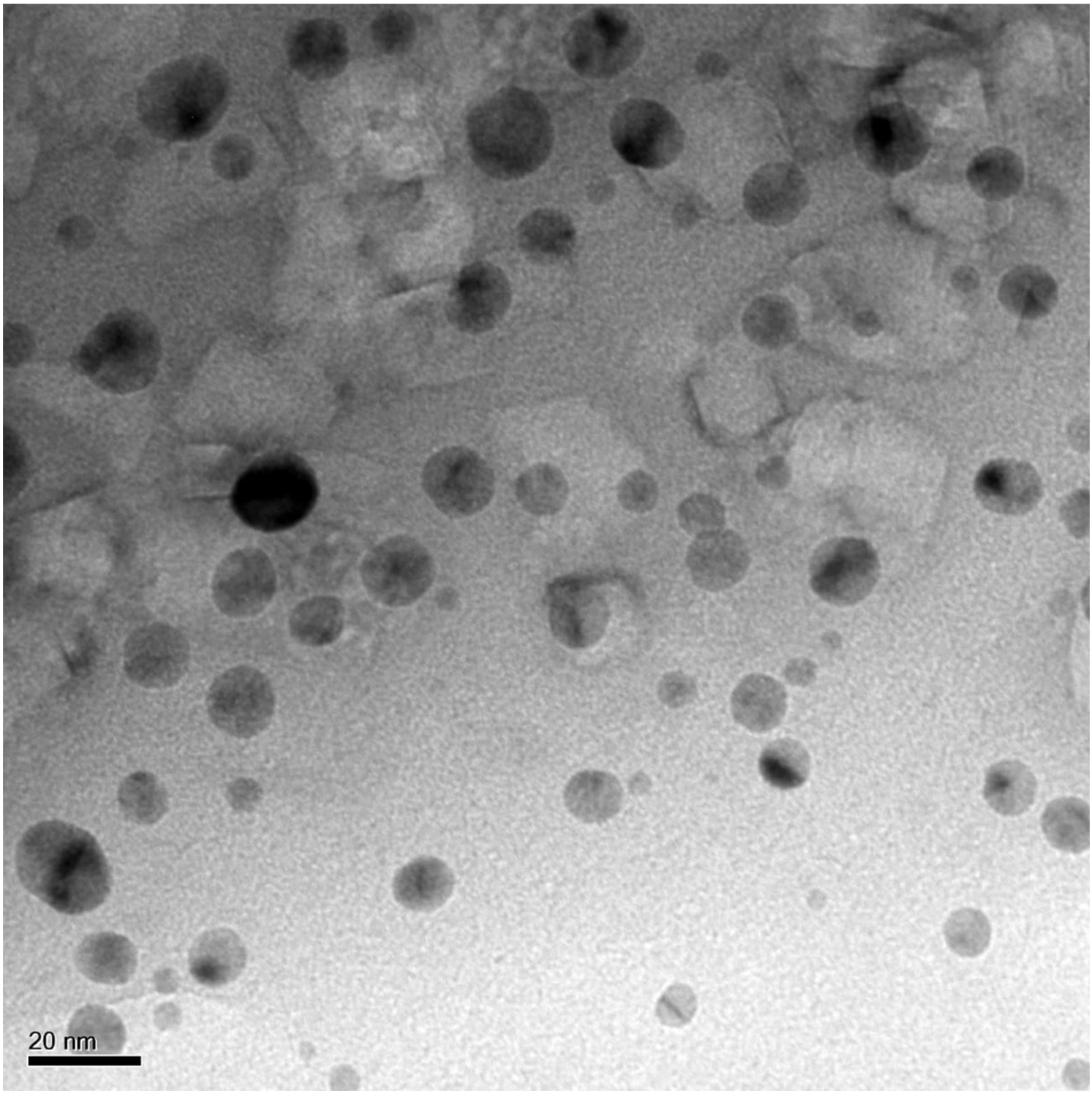

Figure 7

TEM micrographs of Pa-AgNPs

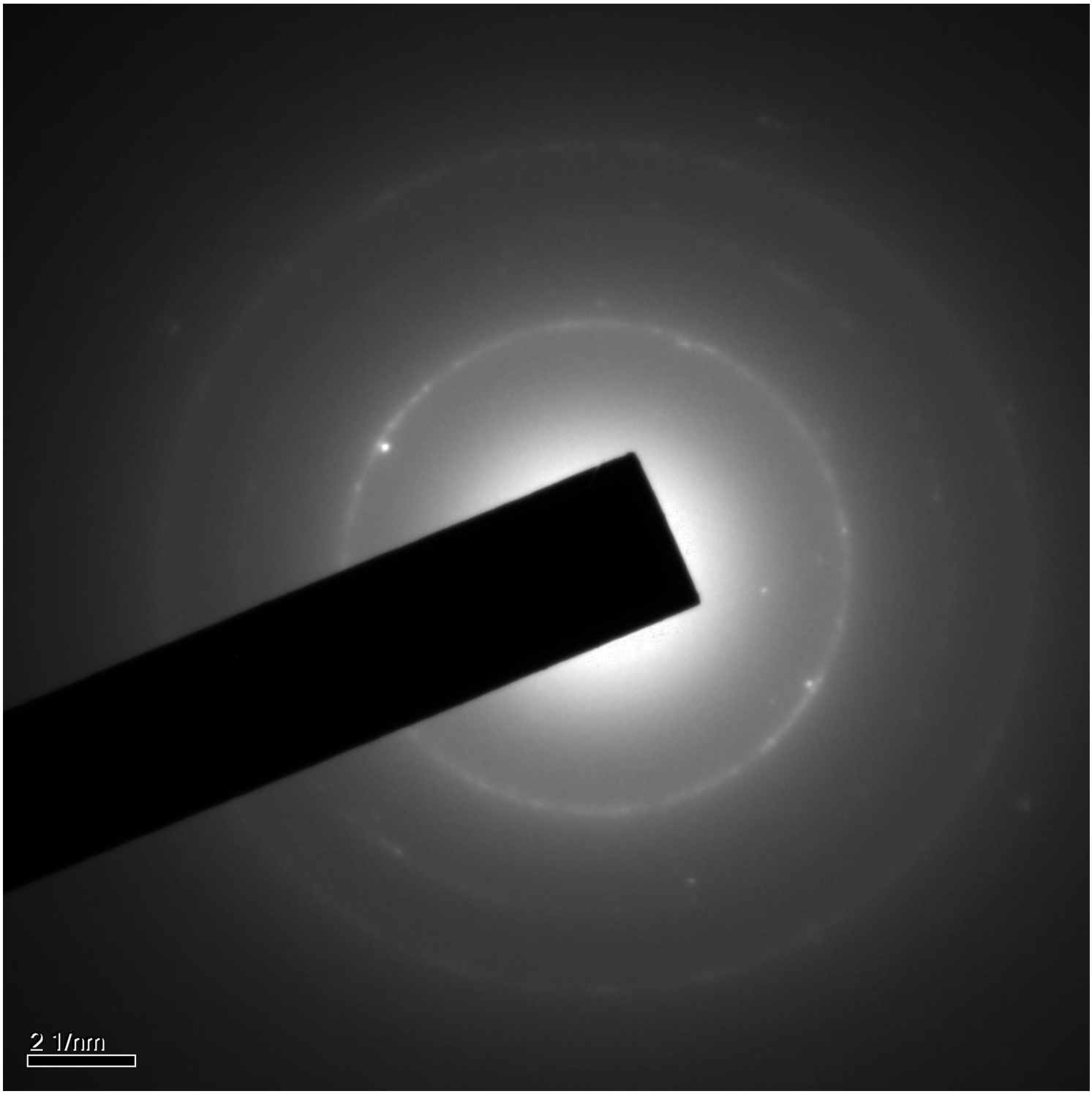

Figure 8

SAED pattern of Pa-AgNPs

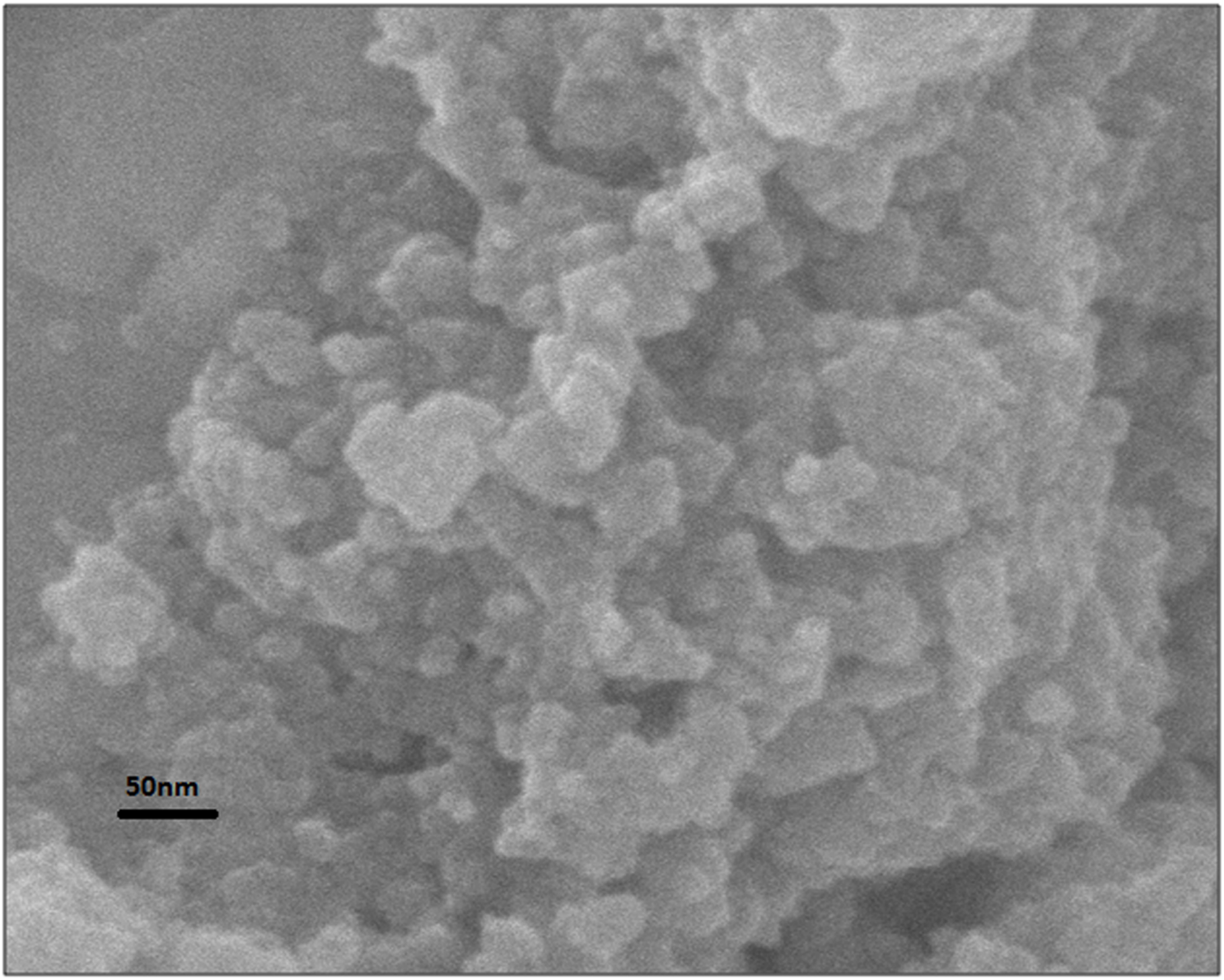

Figure 9

SEM image of Pa-AgNPs

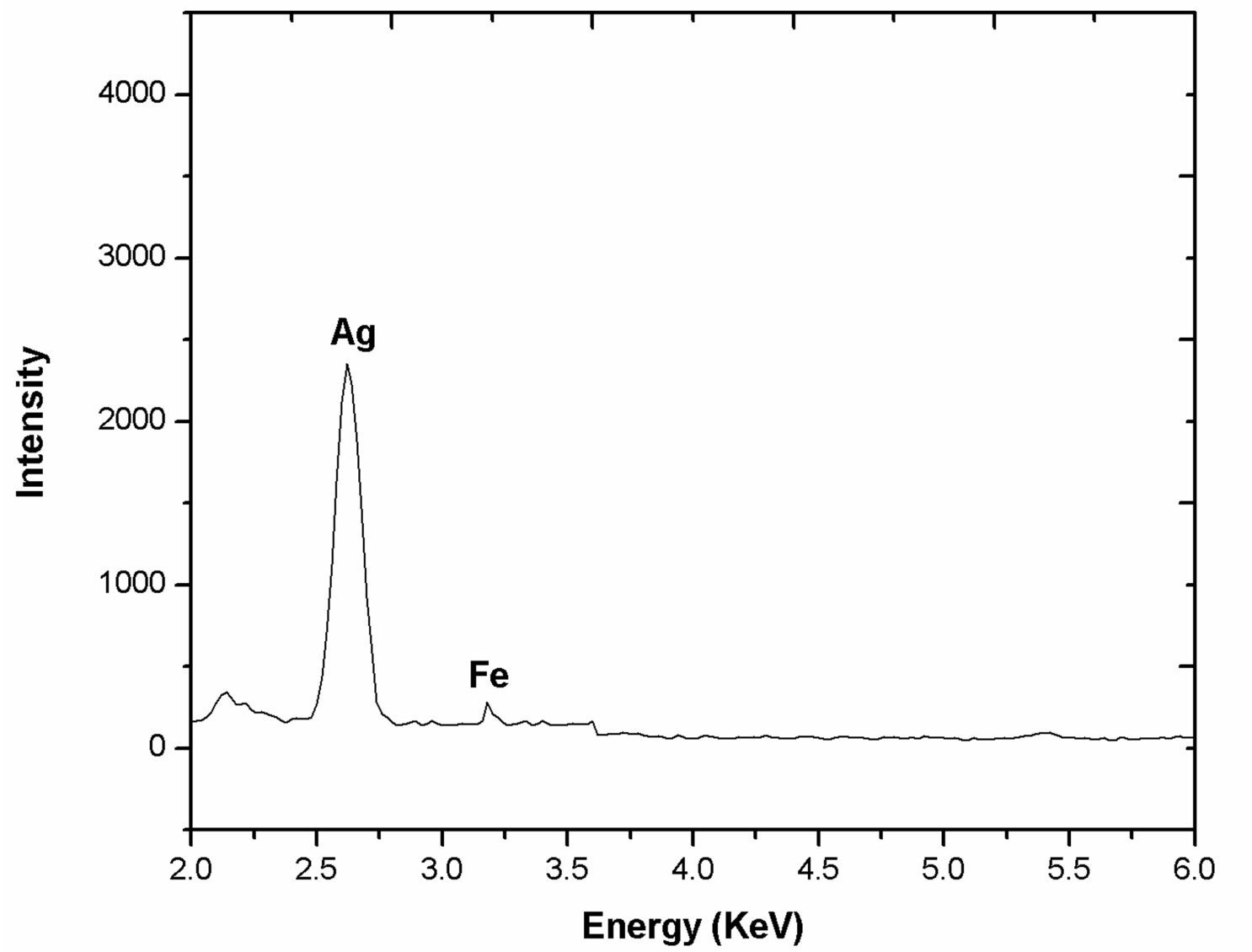

Figure 10

EDX profile of Pa-AgNPs

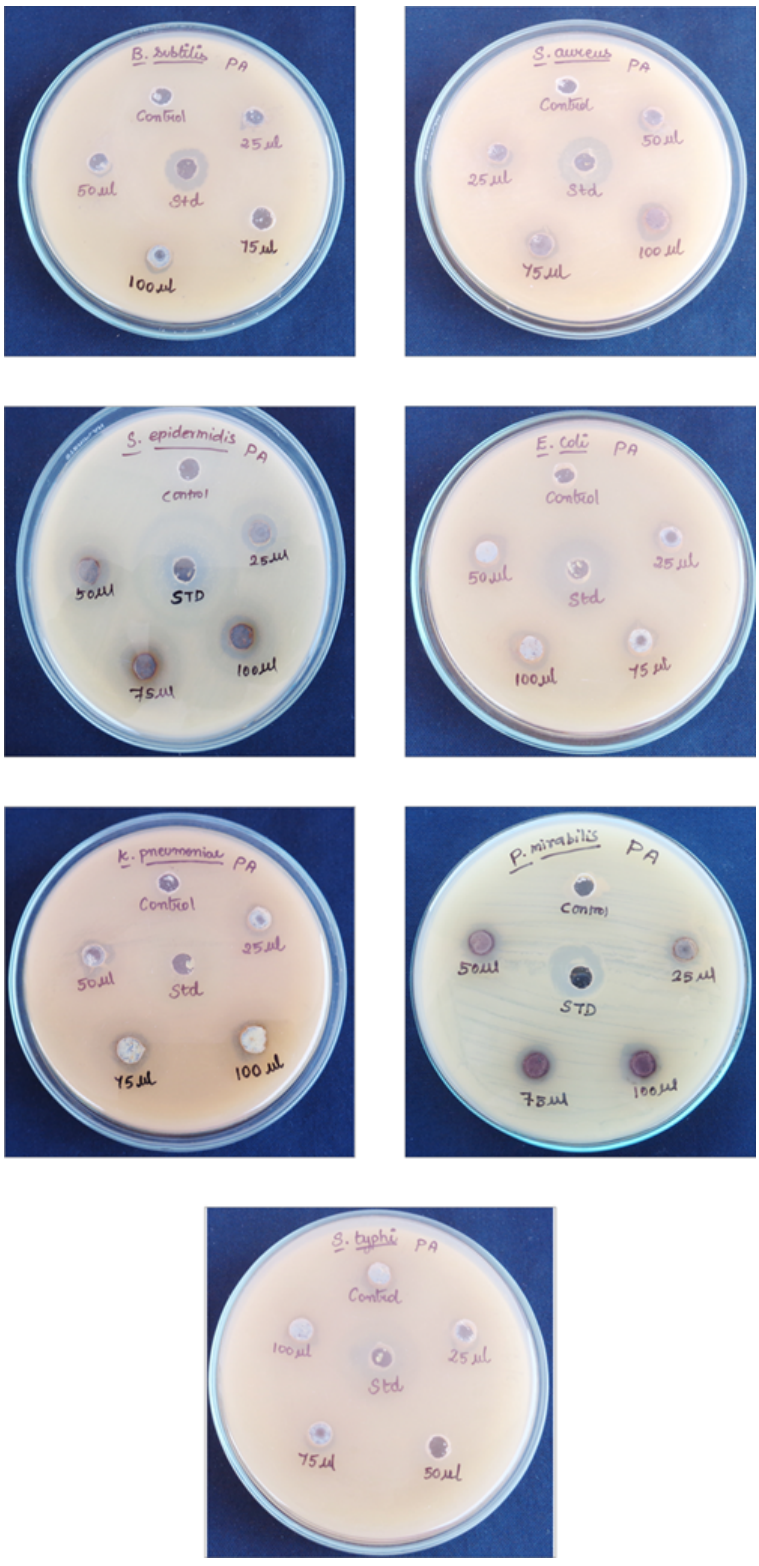

Figure 11

Antibacterial activity of Pa-AgNPs

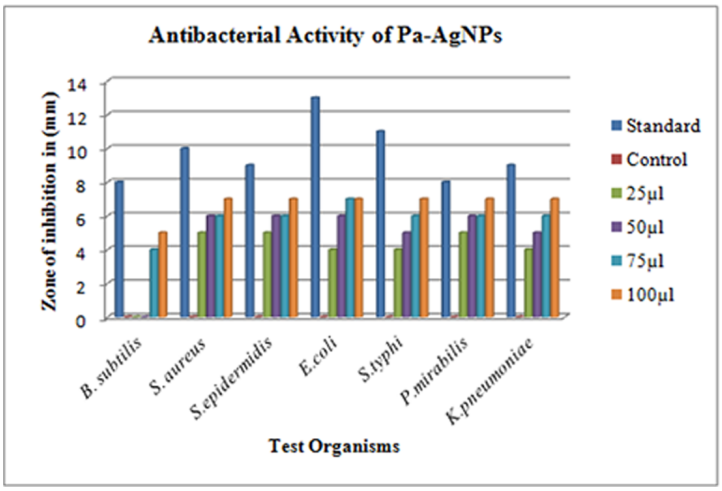

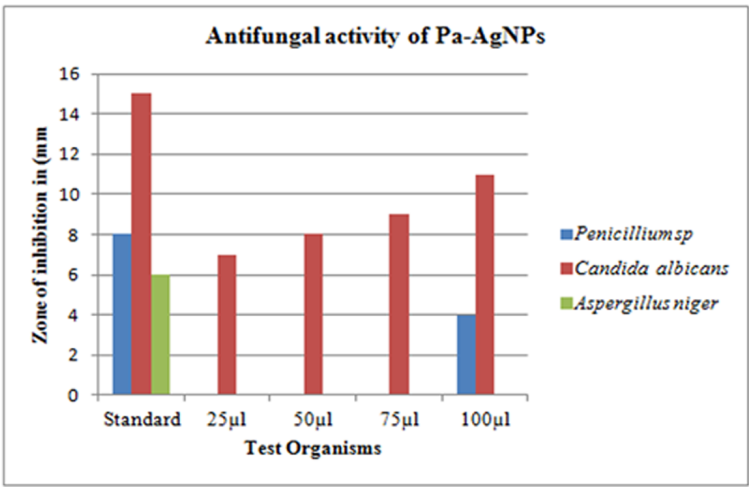

Figure 12

ZOI for the tested pathogens

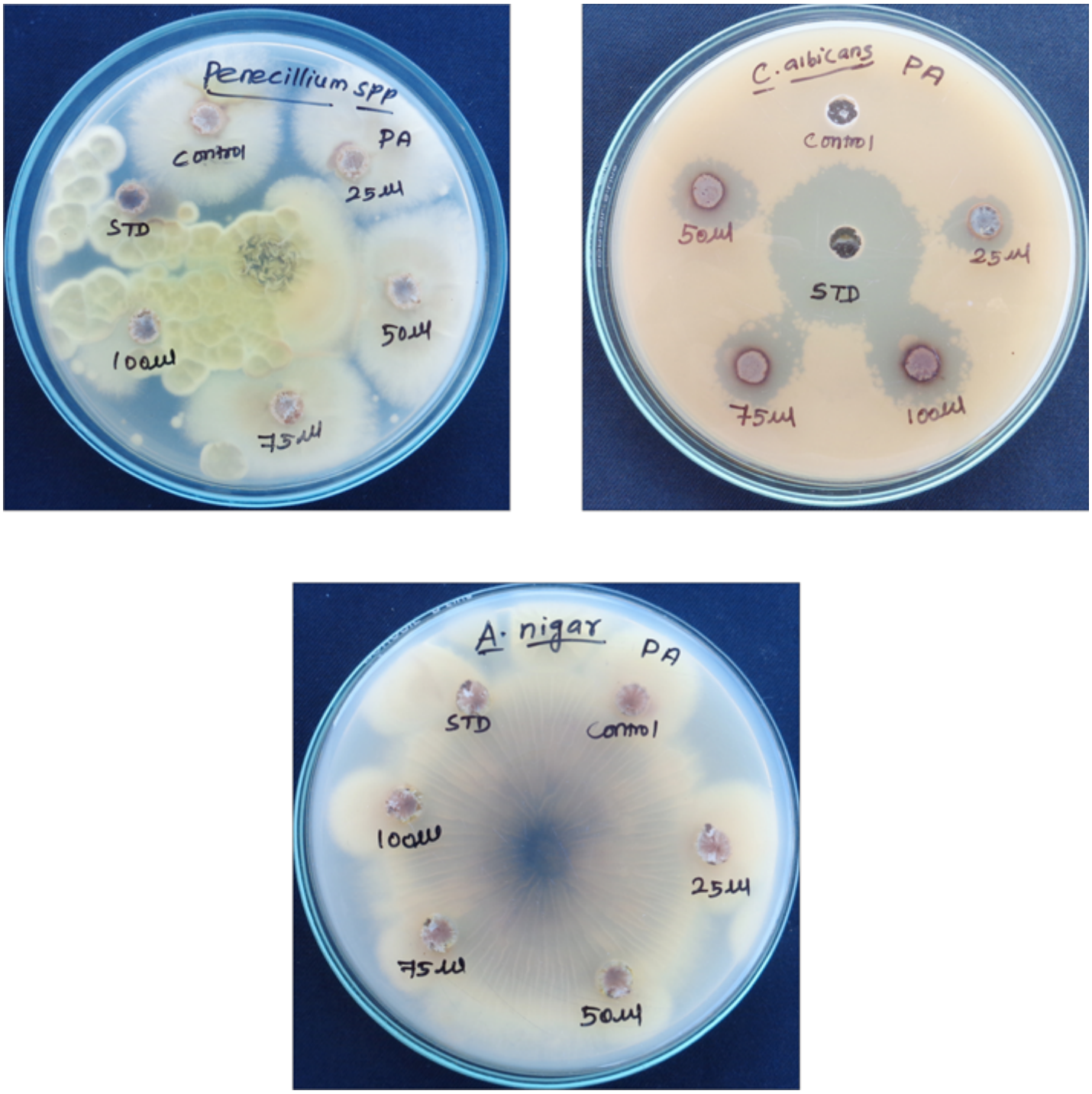

Figure 13

Antifungal activity of Pa-AgNPs

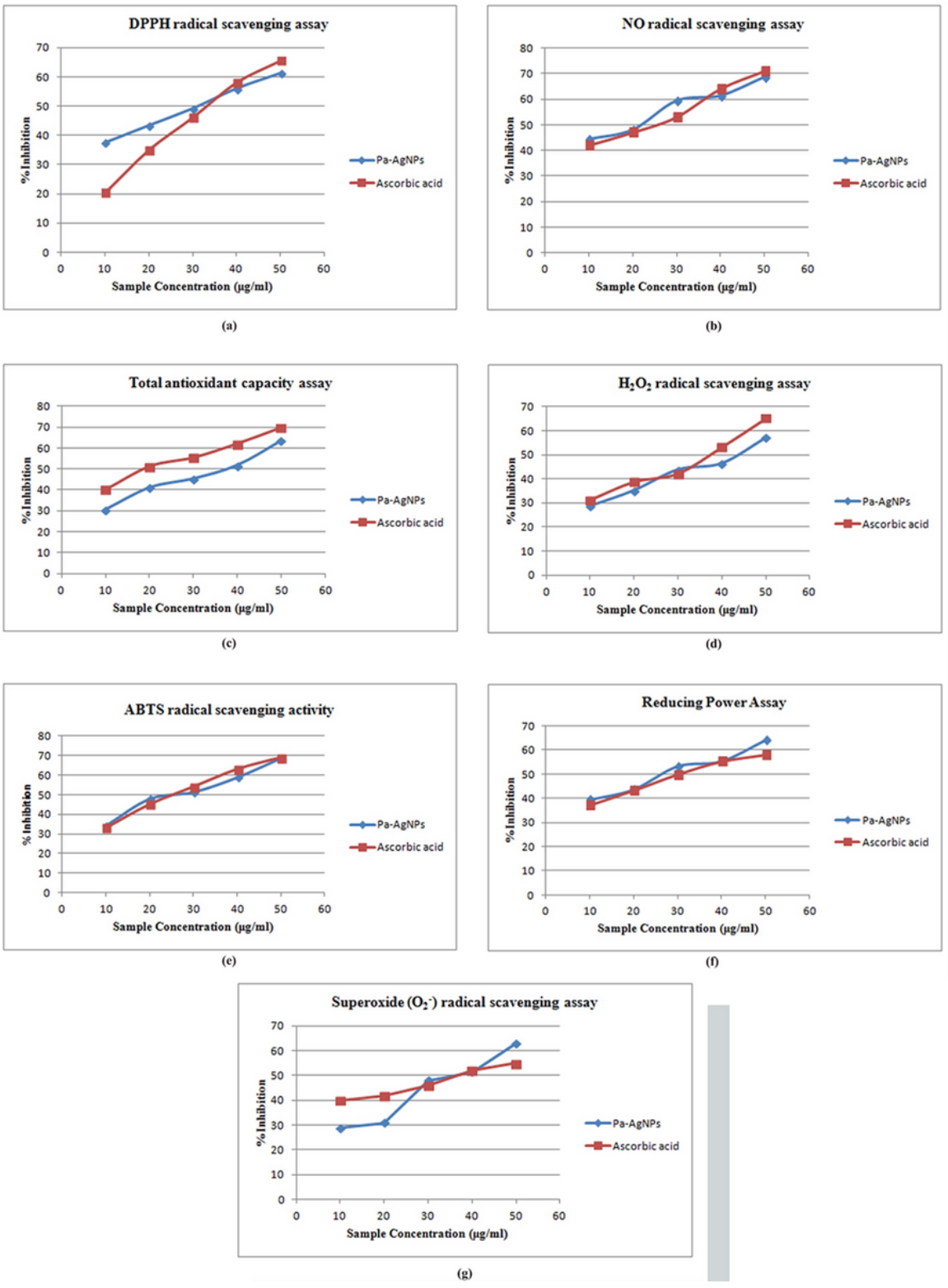

Figure 14

Antioxidant efficacy of Pa-AgNPs